Cluster transport induced by a thermal gradient on a crystalline surface

A. Roux, Nicolas Combe

Cluster transport induced by a thermal gradient on a crystalline surface

A. Roux, N. Combe

Centre d'Elaboration de Matériaux et d'Etudes Structurales, CNRS UPR 8011, 29 rue J. Marvig, BP 94347, 31400, Toulouse, France

Université de Toulouse ; UPS ; F-31055 Toulouse, France

Abstract

Using molecular dynamic (MD) simulations, we study the thermomigration of small clusters consisting of 2, 3 or 4 atoms on a crystalline surface. After evidencing the thermomigration by analyzing the cluster trajectories, we generalize the thermodynamic integration method to compute a thermodynamic potential driving the probability of presence of the clusters on a substrate submitted to a thermal gradient. The study of this thermodynamic potential allows to disentangle the thermomigration effective force from the stochastic diffusion. We show that the heat of transport characterizing the effective force responsible for thermomigration is the sum of the free energy of the cluster-substrate and cluster internal energies. Finally, an unidimensional kinetic model for the thermomigration is proposed and its results compared to the MD trajectories.

1. Introduction

The motion of particles in a liquid or a gas can be induced by a thermal gradient. This phenomenon, referred as thermodiffusion or thermophoresis has initially been evidenced in liquids by Ludwig and Soret [1, 2], and later in gases by Tyndall and Strutt [3, 4]. By analogy with electromigration, this process is also known as thermomigration in solids. [5].

Thermomigration is involved in many different applications, the most famous one being presumably the fabrication of *pn* junctions through the thermal gradient zone melting method in the transistor industry: the doping of silicon by aluminum is achieved using a thermal gradient [6, 7, 8]. Consequently, due to its industrial significance, thermomigration has been extensively studied in bulk materials [9, 10, 11, 12].

Besides, for a few decades, transporting matter in a control way at the nanoscale has been the focus of many investigations, particularly for synthesizing nanoparticles or nanodevices. Surface thermomigration is a significant mass transport mechanism that can be used for these applications. For example, Schoen et al. [13, 14], using molecular dynamics (MD) simulations predicted the control migration of gold nanoparticles confined in carbon nanotubes toward colder regions under a thermal gradient, a prediction later experimentally confirmed by transmission electron microscopy [15, 16]. In crystal growth, surface thermomigration has recently been employed

Email addresses: auroux@cemes.fr (A. Roux), nicolas.combe@cemes.fr (N. Combe)

to control the growth of single-crystal aluminum nanowires [17], serving as a typical example of nanodevice fabrication through thermomigration-based 3D printing. More recently, the migration of vacancy islands on a Si(111) substrate has been observed by low energy electron microscopy: the velocity of vacancy islands is found to be $0.21 nm.s^{-1}$ in the presence of a temperature gradient of $1.3\ 10^4 K.m^{-1}$ [18, 19].

Though, the fundamental mechanisms driving surface thermomigration are not yet fully understood. The aim of this manuscript is precisely to address some of these mechanisms.

In conductors, the thermal heat flux is mainly related to the free electrons motion while phonons play a minor role: hence, surface thermomigration in conductor is closely related to electromigration. Conversely, in this manuscript we focus on semiconductors and insulators where phonons are the primary heat carriers. In these materials, the surface thermomigration involves the interaction between the atoms of the moving object with those of the surface. The surface thermomigration in insulators has been numerically investigated studying nanotubes [20, 21, 22], fullerene or small particles inside nanotubes [23, 24, 25]. The migration of nano-clusters on surfaces (noticeably graphene) has also been highlighted in various theoretical and numerical studies [26, 27, 28, 29, 30]. Beyond, exploiting surface thermomigration between two heat bathes, several authors have imagined nanomachines devices and numerically demonstrated their operations [31, 32, 33, 34].

Quantitatively, the theoretical framework for thermomigration was established by Onsager in the early 1930s [35]. The flux density of particles in a thermal gradient reads

$$\vec{j} = -\frac{DcQ^*}{k_B T^2}\vec{\nabla T} \tag{1}$$

where Q^* is the heat of transport, D the diffusion coefficient, c the particles concentration, and k_B the Boltzmann constant.

Within the scientific community, various mechanisms operating during surface thermomigration have been proposed to relate the heat of transport Q^* to atomic physical properties. Huntington [5] identified several physical mechanisms potentially responsible for the thermomigration: (i) an intrinsic effective driving force [36, 37] independent of the heat carriers, and (ii) a force associated with the transfer of momentum from phonons. While recent studies have suggested that phonon momentum transfer is responsible for the ballistic thermophoresis of clusters on graphene [28], Huntington argued that the intrinsic driving force is dominant in common solids, corresponding to a temperature effect independent of the phonons' direction or nature. Based on Huntington arguments, the coefficient Q^* has been initially related to a migration energy i.e. the activation energy of the diffusion [38, 39, 36, 40, 41, 37].

Recently, studying the surface thermomigration of adatom using MD simulations, we showed that the heat of transport is related to the binding energy of the adatom with the substrate and not to its migration energy [42, 43, 44].

In this paper, we extend our former study on surface thermomigration of adatom to the case of small clusters. Unlike adatoms, clusters have not only a binding energy with the substrate but also an internal energy. These two independent characteristic energies can be modulated by a lattice mismatch between the cluster and the substrate. We show that for clusters the heat of transport corresponds to the sum of the binding and internal energies.

After the description of the model in Sec. 2, we provide few useful characteristics of clusters diffusion on a surface with a homogeneous temperature in Sec. 3. In Sec. 4.1, analyzing cluster trajectories, we evidence the thermomigration and show that the cluster motion involves both a thermal-gradient-induced drift and a Brownian diffusive motion. In Sec. 4.2, we develop a

thermodynamic integration scheme to measure a thermodynamic potential controlling the probability of presence of the cluster. From this potential, we decorrelate the thermal-gradient-induced response from the Brownian diffusion process. Especially, we show that the heat of transport Q^* both depends on the binding energy of the cluster with the substrate and of its internal energy. Finally, in Sec. 5, we propose a kinetic model of the cluster thermomigration and compare it to trajectories derived from MD simulations.

2. System and Methods

In order to simulate the thermomigration of a cluster on a crystalline surface subjected to a thermal gradient, we perform MD simulations: indeed, heat transport by phonons typically involves timescales related to the Debye frequency, a timescale fully handled by MD simulations. We use the LAMMPS simulations package [45].

2.1. Molecular Dynamics

Since we are concerned with the elementary mechanisms of the thermomigration independently of the precise details of the atomic potential, we use a generic model. Interatomic interactions are modeled using a Lennard-Jones [46] (LJ) potential which presents the advantage to minimize the computational cost, while allowing to catch the physical mechanisms underlined by thermomigration. The choice of a LJ potential is rather common in the literature to investigate thermomigration [47, 27, 28, 42]. The interactomic potential involves three type of binding: $\epsilon_{sub-sub} = 1.0$, $\sigma_{sub-sub} = 1.0$ between substrate atoms (atomic mass $m_{sub} = 1.0$), $\epsilon_{cl-cl} = 5.0$, $\sigma_{cl-cl} = 1.0$ between cluster atoms (atomic mass $m_{cl} = 1.0$), and $\epsilon_{cl-sub} = 0.82$, $\sigma_{cl-sub} = 1.0$ between the cluster atoms and the substrate atoms. A 3.5 $\sigma_{sub-sub}$ cut-off distance is applied. Below all quantities will be given in LJ units [48]: distances, masses, energies, times, and temperatures are expressed respectively in units of $\sigma_{sub-sub}$, m_{sub}, $\epsilon_{sub-sub}$, $\sqrt{\frac{m_{sub}\sigma_{sub-sub}}{\epsilon_{sub-sub}}}$ and $\frac{\epsilon_{sub-sub}}{k_B}$. Note that within this choice of units, the Boltzmann constant $k_B = 1$.

Figure 1 reports a sketch of the simulation cell. The substrate is a cubic faced centered crystal. Clusters diffuse on the (111) free surface of the substrate (the z-direction corresponds to the [111] crystalline direction). Periodic boundary conditions are applied in the x and y directions, respectively corresponding to the $[1\bar{1}0]$ and $[11\bar{2}]$ crystalline directions. The substrate sizes along the x, y and z direction are respectively 112.30, 21.55, and 26.13. Within these choices, the simulation box typically contains about 63800 atoms. Cell sizes choice results from a compromise between an affordable computational time and a sufficiently large size to observe the cluster diffusion and to avoid any spurious effects from the quantification of the phonon energies.

The choices of the interatomic potential parameters warrant the absence of dissociation of the cluster, atom evaporation from the substrate and atomic exchange mechanisms during diffusion on the simulation timescale. Especially, our choice of cluster-cluster interatomic energy is artificially high: on one hand, this choice warrants that cluster atoms do not dissociate to release adatoms on the simulation timescale, on the other hand this choice amplifies the potential elastic energy store in the cluster when we will apply a lattice mismatch between the cluster and the substrate. Therefore, the role of elasticity on the thermomigration will be easier to evidence.

2.2. Thermal gradient and temperature profile

In order to apply a thermal gradient, a hot and a cold regions in the substrate (Fig. 1), with thickness 11.2 and spaced by a distance 44.9 are respectively thermostatted at T_{hot} and T_{cold}

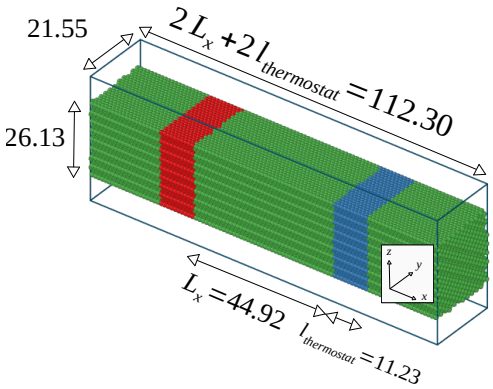

Figure 1: Sketch of the simulation model used to investigate the thermomigration. Atoms in the hot(red) and cold(blue) regions are coupled to Nosé-Hoover thermostats at temperatures T_{hot} and T_{cold}.

using a Nosé-Hoover thermostat (NVT ensemble). The motion of all other atoms of the cell (included the clusters ones) follows the standard Newton equations (microcanonical ensemble or NVE). MD simulations are performed in order to reach a steady state characterized by linear opposite variations of the Nosé-Hoover Hamiltonians of the hot and cold regions. In the following, $T_{hot} = 0.3$ [1] and T_{cold} varies from 0.05 to 0.15 to investigate various thermal gradient. These parameter choices correspond to extremely high thermal gradients: for example, transposing the LJ parameters to a real material such as copper [50] (for which $\epsilon = 0.4096$ eV and $\sigma = 0.2338$ nm and $m = 105.49\ 10^{-27}$ kg) results in a thermal gradient of about 113 $K.nm^{-1}$ for the smallest value of $T_{cold} = 0.05$.

Figure 2 shows the temperature profile along x in the substrate for various thermal gradients. Temperatures profiles are measured from the average kinetic energy per atom $< E_k >$ of 20 slabs of thickness 3.4 evenly distributed between the hot and cold regions. Using the equi-partition theorem, the temperature reads $T = \frac{2}{3} < E_k >$. Both the time average temperature $< T >$ and its standard deviation σ_T are measured and reported on Fig 2.

In Fig. 2, the temperature profiles between the hot and cold regions are linear in agreement with the standard Fourier law for small thermal gradients. For high thermal gradients, weak deviations from the linear behavior are observed that we attribute to a partial ballistic thermal transport. Indeed, measuring the phonon mean free path in the substrate from the thermal conductivity size dependence [51], we find that the phonon mean free path is 26.96, a value comparable to the x-size of the simulation cell [44]. Thus, the thermal transport is partially ballistic in agreement with the nonlinear temperature profile [52]. Though, the typical size of the clusters whose thermomigration will be investigated below is about an order of magnitude smaller than the phonon mean free path: the partial ballistic nature of the thermal transport along the substrate is thus expected to have no effect on the thermomigration mechanism.

Furthermore, Fig. 2 shows some discontinuities of temperatures at the interfaces between the NVE and thermostated (hot or cold) regions: we attribute these discontinuities to the existence of interface resistances or Kapitza resistances [53, 54].

Due to the presence of these Kapitza resistances and to the non-linear temperature profile, there is a slight difference between the temperature variation per unit length $\frac{\Delta T}{L_x} = \frac{T_{hot} - T_{cold}}{L_x}$ and

[1] The fusion temperature of the substrate is $T_f \approx 0.69$ [49]

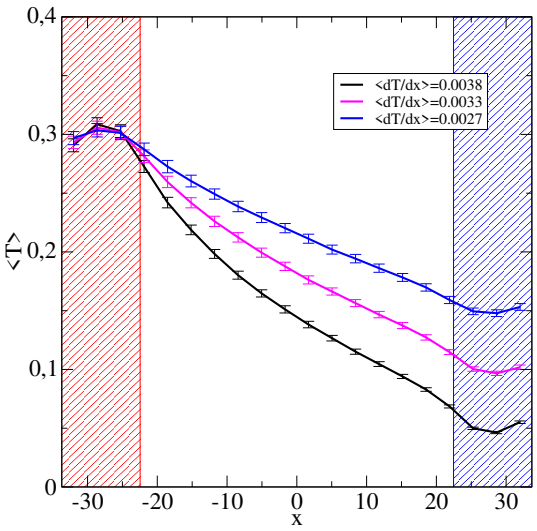

Figure 2: Temperature profiles (and standard deviations) in the substrate. The thermostated regions are indicated by the hatched areas.

Table 1: Average thermal gradient $\langle \frac{\partial T}{\partial x} \rangle$ as a function of the heat baths temperatures T_{cold} and T_{hot}.

T_{hot}	T_{cold}	$\langle \frac{\partial T}{\partial x} \rangle$
0.3	0.05	0.0038
0.3	0.1	0.0033
0.3	0.15	0.0027

the average thermal gradient $\langle \frac{\partial T}{\partial x} \rangle = \frac{1}{L_x} \int_0^{L_x} \frac{\partial T}{\partial x} dx$ extracted from the temperature profile. Thus, below, the thermal gradient will be characterized by the average thermal gradient $\langle \frac{\partial T}{\partial x} \rangle$ whose values as a function of T_{cold} are listed in Table 1.

3. Characteristic of cluster diffusions

3.1. Cluster Sizes and conformations

We investigate the thermomigration of clusters consisting of $N = 2$, $N = 3$ and $N = 4$ atoms.

Figure 3(a) to (c) show snapshots of these clusters (orange atoms) containing respectively $N = 2$, $N = 3$ and $N = 4$ atoms on the substrate (green atoms): these images evidence the equilibrium conformation of the clusters on the surface. Additionally, we have attempted to study clusters containing more atoms [44]. . However, the description of the kinetics of their diffusion or thermomigration is made considerably more difficult by the fact that these later can adopt different conformations on the substrate. For these reasons, we will dedicate the more complex situations to a future publication and concentrate on the simplest cases involving cluster with $N = 2$, $N = 3$, and $N = 4$ in this work.

Before investigating the thermomigration of these clusters, we characterize their diffusion on a substrate at homogeneous temperature T.

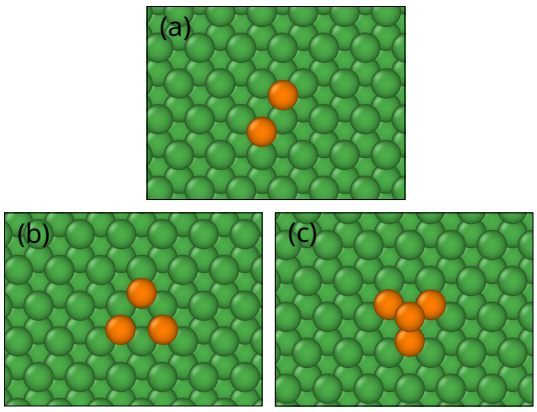

Figure 3: Snapshots (top-view) of the clusters (in orange) with $N = 2$, $N = 3$ and $N = 4$ atoms on the substrate surface.

3.2. Cluster diffusion characteristics

Performing MD simulations on a substrate at uniform temperature $T \in [0.1 - 0.3]$, we measure the mean square displacement (MSD) of the clusters $MS\,D(\tau) = \left\langle (\vec{r}(t+\tau) - \vec{r}(t))^2 \right\rangle$ with $\langle\rangle$ the time average and $\vec{r}(t)$ the position of the cluster's center of mass (COM). Plotting $MS\,D(\tau)$ in a log-log plot, we have checked that the diffusion of the cluster is normal $MS\,D(\tau) \propto \tau$ which allows us to evaluate a diffusion coefficient.

For each cluster size, the diffusion coefficient follows an Arrhenius law $D(T) = D_0\, e^{-\frac{E_a}{k_B T}}$. A regression provides the diffusion activation energy E_a and the prefactors D_0 that we report in Table 2. For comparison, we also report in Table 2 those found for a diffusing adatom [42].

For $N = 2$ and $N = 3$, the cluster diffusion activation energy E_a is roughly the number of atoms in the cluster times the diffusion activation energy of an adatom. Indeed, for $N = 2$ and $N = 3$, all atoms are in contact with the substrate. Besides, for $N = 4$, the diffusion activation energy E_a of a 4 atoms cluster is roughly three times the activation energy for diffusion of an adatom: a 4 atoms cluster has a pyramid-like conformation with 3 atoms in direct contact with the substrate (see Fig. 3(c)), in agreement with the measured activation energy E_a.

Table 2: Diffusion activation energy E_a, prefactors D_0 and ratio $\frac{E_a}{E_a(N=1)}$ of the activation energy by the adatom activation energy as a function of clusters sizes.

N	E_a	Do	$\frac{E_a}{E_a(N=1)}$
1	0.287	0.227	1
2	0.617	0.419	2.150
3	0.838	0.504	2.920
4	0.884	0.528	3.080

3.3. Lattice mismatch and cluster diffusion

In order to address the effect of the lattice mismatch on the cluster diffusion coefficient, we perform MD simulations and analyze the cluster trajectories on a substrate at homogeneous temperature $T = 0.25$ varying the parameter σ_{cl-cl} between $\sigma_{cl-cl} \in [0.6, 1.12]$. Computing the

MSD, we deduce the cluster diffusion coefficient that we plot in Fig. 4(a) as a function of the distance σ_{cl-cl} for different cluster sizes.

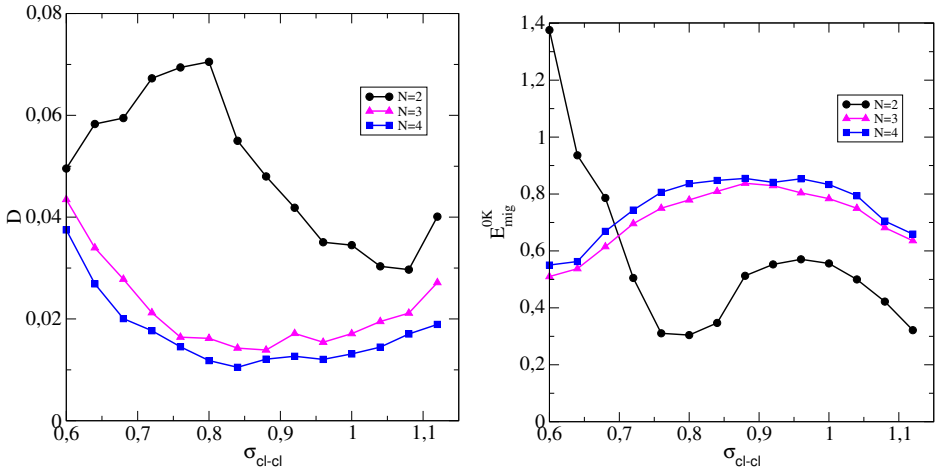

Figure 4: (a) Diffusion coefficient as a function of the distance σ_{cl-cl} for different cluster sizes at $T = 0.25$. (b) Migration energies E^{0K}_{mig} at 0 K as a function of the distance σ_{cl-cl} for different cluster sizes.

In order to understand the origin of the variation of the diffusion coefficient, we have computed the cluster migration energy E^{0K}_{mig} shown in Fig. 4(b) as a function of the distance σ_{cl-cl}. The migration energy E^{0K}_{mig} is defined here as the amplitude of the energy $E^{OK}(x)$ as a function of the x-position of the COM of the cluster. $E^{OK}(x)$ is obtained by minimizing the energy of the system (cluster+substrate) constraining the x-position of the COM of the cluster [2]. E^{0K}_{mig} should be equivalent to the diffusion activation energy E_a providing that only one diffusion mechanism operates. For all investigated cluster sizes, the migration energies Fig. 4(b) present variations opposite to those of the diffusion coefficient Fig. 4(a).

For $N = 3$ and $N = 4$ cluster sizes, the diffusion coefficients approximately evolve quadratically with the parameter σ_{cl-cl}. The diffusion coefficient is minimum for $\sigma_{cl-cl} \approx 0.9$. The migration energy presents an opposite variation with a maximum around $\sigma_{cl-cl} \approx 0.85$. A minimum of the diffusion coefficient as a function of the lattice mismatch has already been observed in simulations of cluster diffusion [55, 56]: varying the cluster-substrate lattice mismatch induces an elastic energy in the cluster and a variation of the binding energy of the cluster with the substrate, two quantities to which the migration energy is related.

The behavior of $N = 2$ cluster size is singular compared to the $N = 3$ and $N = 4$ cases, the diffusion coefficient increases up to a maximum for $\sigma_{cl-cl} \approx 0.8$ and then decreases to reach a minimum at $\sigma_{cl-clmin} \approx 1.1$. This variation agrees with the ones of the migration energy. We think that the presence of both a maximum and a minimum of the diffusion coefficient is related to the existence of two diffusion mechanisms for 2 atoms clusters: the cluster can move through translation or rotation. Both mechanisms yield the displacement of the cluster COM but their activation energies differ by a factor of approximately 2.

[2] The y- and -z position of the cluster COM are not constrained.

4. Thermomigration of cluster on a crystalline surfaces

4.1. Cluster Trajectories

For each cluster sizes, we examine 50 trajectories of diffusion on substrate submitted to different thermal gradients: the initial x-position of the cluster COM is at middle distance between the hot and cold regions while its y-position is random. From these 50 trajectories, we compute an average trajectory.

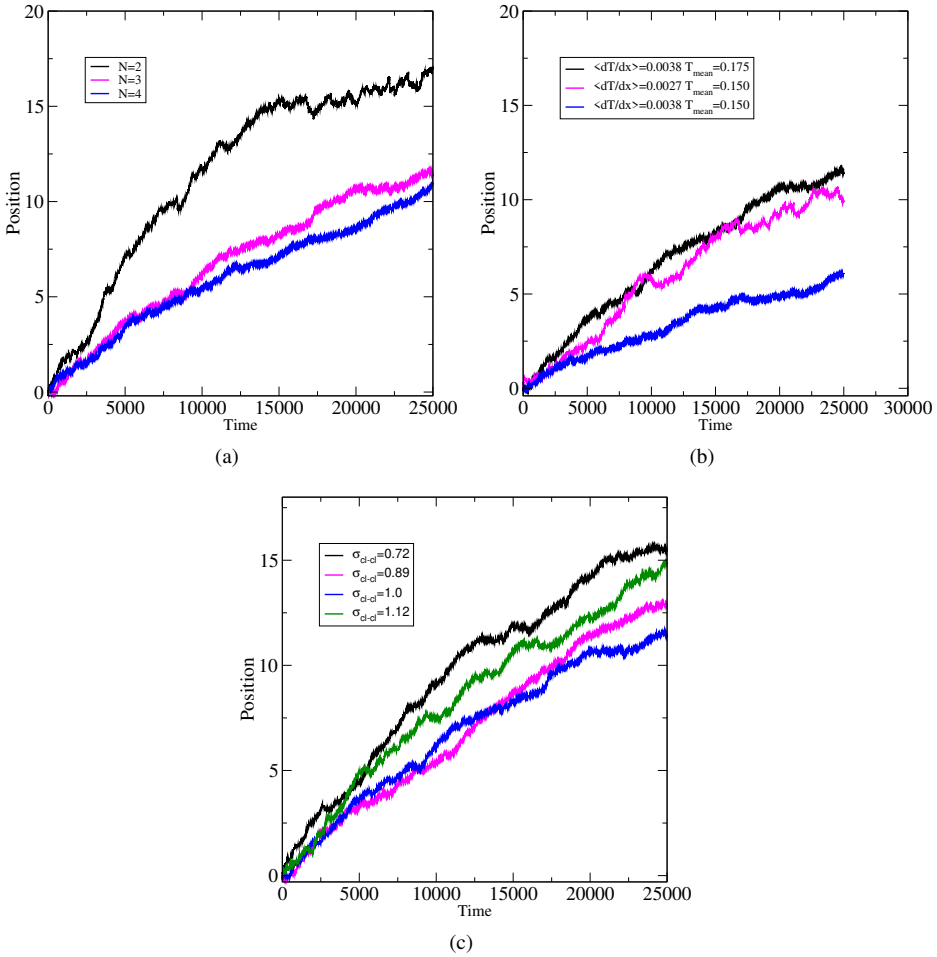

Figure 5: (a) Average trajectories of clusters with $N = 2$, $N = 3$ and $N = 4$ atoms. $\langle \frac{\partial T}{\partial x} \rangle = 0.0038$ and $T_{mean} = 0.175$ and $\sigma_{cl-cl} = 1$. (b) Average trajectories of clusters with $N = 3$ atoms for different mean temperatures $T_{mean} = \frac{T_{hot}+T_{cold}}{2}$ and different thermal gradients $\langle \frac{\partial T}{\partial x} \rangle$. $\sigma_{cl-cl} = 1$. (c) Average trajectories of a 3 atoms cluster as a function of the distance σ_{cl-cl}. $\langle \frac{\partial T}{\partial x} \rangle = 0.0038$ and $T_{mean} = 0.175$.

4.1.1. Cluster size

Figure 5(a) shows the average trajectory for clusters of $N = 2$, $N = 3$ and $N = 4$ atoms. The thermal gradient is set to $\langle \frac{\partial T}{\partial x} \rangle = 0.0038$ and the distance $\sigma_{cl-cl} = 1$. The average trajectory is computed by averaging the x-position of the cluster COM at a given time t over all MD trajectories with the same initial x-position.

Regardless of the number of atoms, the cluster COM moves towards the positive x, i.e. towards the cold region. The thermal gradient induces an effective force on the clusters pushing them towards the cold region. In addition, the cluster migration speed decreases with the cluster size, which is in line with the diffusion coefficients' dependence on cluster sizes (see section 3.2). Finally, the trajectories of clusters display two main ingredients: a thermal gradient induced drift and a random diffusion.

4.1.2. Thermal gradient and local temperature

To investigate the effects of the thermal gradient and of the local temperature, Fig. 5(b) shows the average trajectories of a cluster $N = 3$ for varying hot T_{hot} and cold T_{cold} temperatures corresponding to different thermal gradient $\langle \frac{\partial T}{\partial x} \rangle$ and different mean substrate temperature defined as $T_{mean} = \frac{T_{hot}+T_{cold}}{2}$.

We first compare the trajectories with a fixed mean substrate temperature $T_{mean} = 0.175$. For thermal gradients $\langle \frac{\partial T}{\partial x} \rangle = 0.0038$ and $\langle \frac{\partial T}{\partial x} \rangle = 0.0027$, the trajectories have respectively a mean velocity of $\bar{v} = 4.55\ 10^{-4}$ and $\bar{v} = 3.96\ 10^{-4}$. The mean speed of the cluster is defined here as the average speed $\bar{v}$ between $t = 0$ and $t = 25\ 000$. Hence, while the thermal gradient increases by a factor $\frac{0.0038}{0.0027} = 1.41$, the mean speed increases by a factor 1.15, of the same order of magnitude but slightly smaller. The discrepancy between these two values are presumably due to a lack of statistics in order to evaluate the mean speed and more probably to the naive and rough analysis done here (the average thermomigration speed depends on the thermal gradient and on the local temperature Eq. (1)).

Comparing trajectories with a fixed thermal gradient $\langle \frac{\partial T}{\partial x} \rangle = 0.0038$ in Fig. 5(b), the mean speed for a mean temperature $T_{mean} = 0.175$ is about 1.92 times higher than the one for an average temperature $T_{mean} = 0.150$. This ratio of 1.92 is to be compared with the ratio of the cluster diffusion coefficients at the temperatures $T_{mean} = 0.150$ and $T_{mean} = 0.1750$ computed from data of Table 2: $\frac{D(T=0.175)}{D(T=0.150)} \approx 2.2$ of the order of 1.92. Again, we think that the discrepancy between these values is presumably due to a lack of statistics and to our naive and rough analysis.

4.1.3. Lattice mismatch

Figure 5(c) shows the average trajectory of the $N = 3$ cluster for different σ_{cl-cl} distances for a thermal gradient $\langle \frac{\partial T}{\partial x} \rangle = 0.0038$ and a mean temperature $T_{mean} = 0.175$.

The trajectories for $\sigma_{cl-cl} = 0.89$ and $\sigma_{cl-cl} = 1$ have the lowest mean speed while those for $\sigma_{cl-cl} = 0.72$ and $\sigma_{cl-cl} = 1.12$ the highest. This result is consistent with the cluster diffusion coefficient dependence on σ_{cl-cl} reported in Fig. 4(a).

We conclude that the thermomigration of cluster seems to agree with Eq. (1) but that the trajectory analysis is necessarily limited by statistics.

4.2. Thermodynamic Integration

In order to overcome the trajectories examinations and to quantitatively disentangle the thermal gradient induced drift and the random diffusion, we proposed in our previous work [42, 43]

to generalize the thermodynamic integration (TI) algorithm to the case of system with an inhomogeneous temperature. Our method was designed to determine the thermodynamic potential driving the diffusion of an adatom in the presence of a thermal gradient. In this section, we propose to extend this algorithm to the case of clusters.

4.2.1. Local thermodynamic equilibrium

First, we have investigated the local thermodynamic equilibrium of the clusters in contact with the substrate by measuring the velocity distribution of clusters atoms as a function of the cluster position. The sizes of the clusters investigated here are very small compared to the typical length of variation of the thermal gradient: indeed, for the highest investigated thermal gradient $\langle \frac{\partial T}{\partial x} \rangle = 0.0038$, the temperature varies of 0.004 over the typical sizes of clusters considered here. Figure 6(a) shows the clusters velocity distributions $G(v_y)$ as a function of the y-velocity

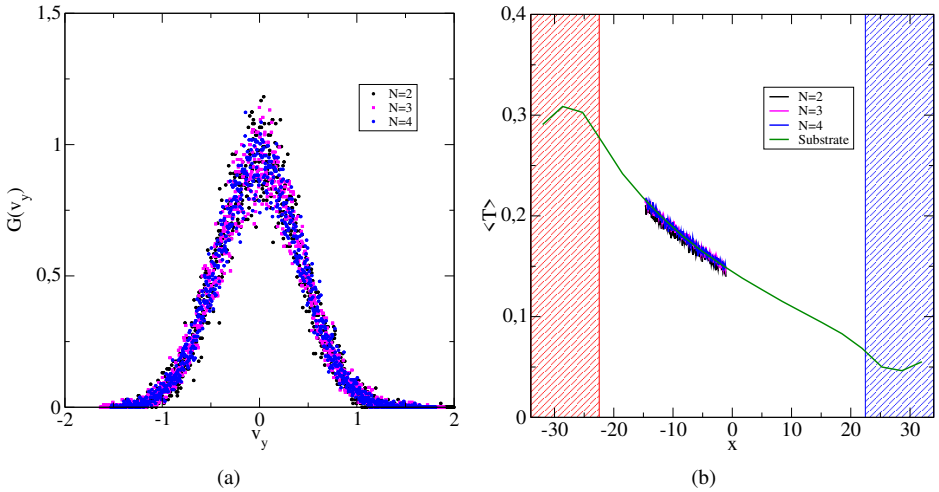

Figure 6: $\langle \frac{\partial T}{\partial x} \rangle = 0.0038$ and $T_{mean} = 0.175$ (a) Velocity distributions of clusters with COM at position $x_0 = -8.81$. (b) Temperature profile of the substrate and clusters temperature evaluated from the velocity distribution along the x axis.

v_y of clusters for a thermal gradient $\langle \frac{\partial T}{\partial x} \rangle = 0.0038$ and $T_{mean} = 0.175$. Velocity distributions are calculated while constraining the x-position of the COM. This distribution fits well with a Maxwell distribution $G(vy) = \sqrt{\frac{m}{2\pi k_B T}}\ e^{-\frac{mvy^2}{2k_B T}}$ and allows to deduce the cluster temperature.

Figure 6(b) compares the temperature profile of the substrate Fig. 2 (evaluated from the equipartition theorem) and the cluster temperatures evaluated from the velocity distributions. Both temperatures agree so that we can reasonably assume that the clusters are in a local thermodynamic equilibrium with the substrate.

4.2.2. Thermodynamic potential and thermodynamic integration

We define the probability $p(x_0)$ to find the cluster with its COM at coordinate x_0 and the associated thermodynamic potential $\Phi(x_0) : p(x_0) \propto exp(-\Phi(x_0))$. Under the local thermodynamic equilibrium assumption, in a system with an inhomogeneous temperature, the thermodynamic potential $\Phi(x_0)$ reads:

$$\Phi(x_0) = -\ln[Z_r(x_0)] \tag{2}$$

$$Z_r(x_0) = \frac{1}{h^{3M+3N}} \int \delta\left(\frac{\sum^M x_k}{M} - x_0\right) e^{\left[-\int \frac{\mathcal{H}(\vec{r})}{T(\vec{r})} d^3\vec{r}\right]} \prod_{k=1}^{M} d^3\vec{r}_k d^3\vec{p_k}^3 \prod_{i=1}^{N} d^3\vec{r}_i d^3\vec{p}_i \tag{3}$$

Where positions $\vec{r_k} = (x_k, y_k, z_k)$ and momentum $\vec{p_k}$ of cluster atoms are denoted with indices k (or l) while substrate atoms coordinates are denoted with the index i (or j). M and N are the numbers of atoms in the cluster and in the substrate. $\mathcal{H}(\vec{r})$ is the microscopic many-body Hamiltonian density of the system defined as [57, 58]:

$$\begin{aligned}\mathcal{H}(\vec{r}) = & \sum_k^M \delta(\vec{r_k} - \vec{r}) \left[\frac{p_k^2}{2m_k} + \frac{1}{2}\sum_i^N E_{LJ}(\vec{r_k}, \vec{r_i}) + \sum_{l\neq k}^M \frac{1}{2} E_{LJ}(\vec{r_k}, \vec{r_l})\right] \\ & + \sum_i^N \delta(\vec{r_i} - \vec{r}) \left[\frac{p_i^2}{2m_i} + \frac{1}{2}\sum_k^M E_{LJ}(\vec{r_k}, \vec{r_i}) + \sum_{j\neq i}^N \frac{1}{2} E_{LJ}(\vec{r_i}, \vec{r_j})\right]\end{aligned} \tag{4}$$

with m_k and m_i the masses of the cluster and substrate atoms.

The direct calculation of the thermodynamic potential $\Phi(x_0)$ is out of our computational capabilities because it would involve an integral over all microstates. However, it is possible to calculate its derivative $\frac{\partial\Phi}{\partial x}$. Appendix A establishes the expression of $\frac{\partial\Phi}{\partial x}$:

$$\begin{aligned}\frac{\partial\Phi}{\partial x}(x_0) = & -\frac{\frac{\partial Z_r}{\partial x_0}}{Z_r}(x_0) \\ = & -\left\langle \sum_i^N \sum_k^M \frac{F_x(i\to k)}{2}\left[\frac{1}{T(x_k)} + \frac{1}{T(x_i)}\right]\right\rangle_{x_0} + \left\langle \sum_k^M \frac{\partial\left(\frac{1}{T(x_k)}\right)}{\partial x_0}\left[\frac{{p_k}^2}{2m} + \frac{E_{LJ}(k\leftrightarrow sub)}{2}\right]\right\rangle_{x_0} \\ & + \left\langle \sum_k^M \sum_{l\neq k}^M \frac{1}{2}\frac{\partial\left(\frac{1}{T(x_k)} + \frac{1}{T(x_l)}\right)}{\partial x_0} E_{LJ}(k\leftrightarrow l)\right\rangle_{x_0}\end{aligned} \tag{5}$$

where $\langle . \rangle_{x_0}$ denotes an average over all microstates compatible with the x-position x_0 of the cluster COM. $F_x(i \to k)$, $E_{LJ}(k \leftrightarrow sub)$ and $E_{LJ}(k \leftrightarrow l)$ are respectively the x-component of the force exerted by atom i on atom k, the interaction energy between the cluster and the substrate and the internal energy of the cluster.

While the first right-hand term of Eq. (5) is standard in TI implementation (in homogeneous temperature systems), the second and third terms derived from the presence of the thermal gradient. In order to compute the thermodynamic potential, we develop and implement a user-command to the LAMMPS code that evaluates Eq. (5).

4.2.3. Thermodynamic potential

We perform MD simulations similar to a thermodynamic integration method: we constrain the x-coordinate of the cluster COM to compute $\frac{\partial\Phi}{\partial x}(x_0)$ using Eq. (5) from which we deduce Φ by numerical integration. Figure 7(a) shows the thermodynamic potential $\Phi(x_0)$ as a function of the position of the COM for a cluster $N = 3$ for three thermal gradients. The potential $\Phi(x_0)$ is the sum of a decreasing function referred as ϕ_{TGIP} and a periodic function ϕ_{Diff}. We define

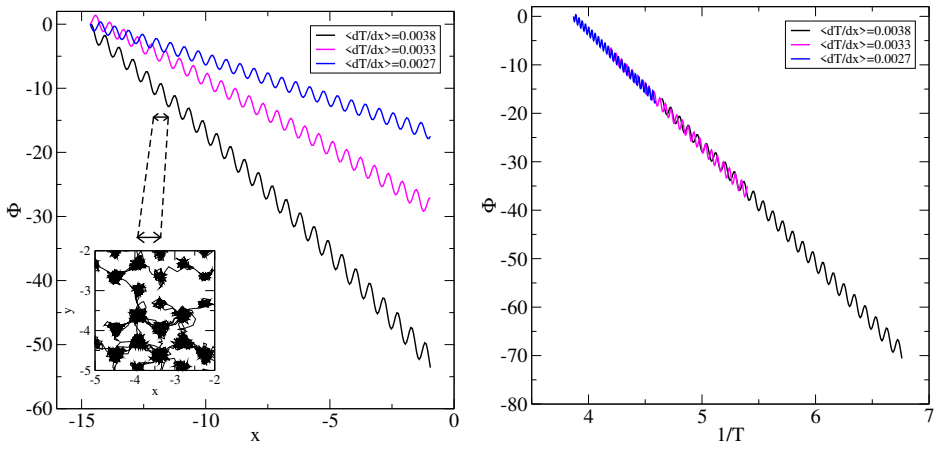

Figure 7: Thermodynamic potential of the $N = 3$ cluster for several thermal gradients $\langle \frac{\partial T}{\partial x} \rangle$. (a) Thermodynamic potential $\frac{\partial \Phi}{\partial x}(x)$ as a function of the position x of the cluster's COM. The inset in Fig. 7(a) shows the successive positions (x,y) of the center of mass of a diffusing cluster on the (111) surface. The distance a_x between two stable sites on the surface in the x direction is $a_x \approx 0.56$. (b) Thermodynamic potential Φ as a function of the inverse of temperature $\frac{1}{T)}$.

ϕ_{TGIP} as the curve passing through all minima of the thermodynamic potential. The potential ϕ_{TGIP} characterizes the thermomigration : its derivative corresponds to an effective force driving the cluster towards the cold region: the cluster's probability of presence $p(x_0)$ increases with decreasing temperature.

Using the temperature profile Fig. 2, the thermodynamic potential is plotted in Fig. 7(b) as a function of the inverse of the temperature $\frac{1}{T}$. Within this choice of coordinates, the potential ϕ_{TGIP} coincides for all thermal gradients. In addition, the function $\phi_{TGIP}(\frac{1}{T})$ is quasi-linear.

Conversely, the function ϕ_{Diff} characterizes the diffusion of the cluster on the substrate: the inset of Fig. 7(a) shows the trajectory of the cluster COM evidencing the crystallography of the surface consistent with the period of the function ϕ_{Diff}.

4.2.4. Interpretation of thermodynamic potential

To interpret the thermodynamic potential, we use the expression Eqs. (2) and (3). The microscopic many-body Hamiltonian density $\mathcal{H}(\vec{r})$ involves three types of energies: the substrate-substrate $\mathcal{H}sub - sub$, the cluster-cluster $\mathcal{H}_{Cl-Cl}$ and the cluster-substrate $\mathcal{H}_{Cl-sub}$ energies. Among them, the cluster-cluster and cluster-substrate energies involve the COM of the cluster while $Esub - sub$ weakly depends on x_0 for x_0 corresponding to metastable position of the cluster. Thus, in order to interpret Eqs. (2) and (3), we note that under the condition $\frac{\sum^M x_k}{M} - x_0 = 0$ and x_0 corresponding to metastable position of the cluster:

$$\int \frac{\mathcal{H}(\vec{r})}{T(\vec{r})} d^3\vec{r} \approx \frac{E_{Cl-Cl}}{T(x_0)} + \frac{E_{Cl-sub}}{T(x_0)} + \int \frac{\mathcal{H}_{sub-sub}(\vec{r})}{T(\vec{r})} d^3\vec{r} \tag{6}$$

Where E_{cl-sub} and E_{cl-cl} are the cluster-substrate binding and cluster internal free energies. Combining Eqs. (6) and (2), we conclude that the minima of thermodynamic potential should vary

following

$$\Phi(x_0)|_{min} \approx -\frac{E_{cl-sub} + E_{cl-cl}}{T(x_0)} + ... \tag{7}$$

This relation agrees with results of Fig. 7(b) evidencing a linear relationship of the potential ϕ_{TGIP} as a function of $\frac{1}{T}$. Below, we will show this agreement is not only qualitative but also quantitative.

The interpretation Eq. (7) is quite natural, since by considering an infinitely small thermal gradient, one should recover the probability of cluster presence on a substrate at homogeneous temperature T: $P(x_0) \propto e^{-\frac{A(x_0)}{T(x_0)}} \Pi_{sub-sub}$ with $A(x_0)$ the cluster-substrate binding and cluster internal free energy of the cluster constrained at abscissa x_0 and $\Pi_{sub-sub}$ a function mainly depending on substrate-substrate interaction independent on x_0.

4.3. Thermomigration characterization

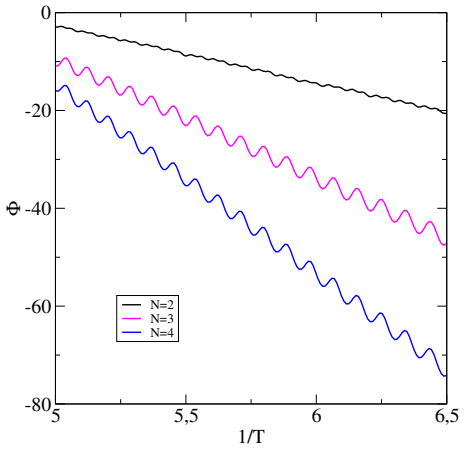

Figure 8: Thermodynamic potential for several clusters sizes as a function of inverse temperature $\frac{1}{T}$. The potential is measured for a substrate subjected to a thermal gradient $\langle \frac{\partial T}{\partial x} \rangle = 0.0038$.

4.3.1. Thermal gradient induced drift

Figure 8 shows the thermodynamic potential as a function of inverse temperature for different clusters sizes and for a thermal gradient $\langle \frac{\partial T}{\partial x} \rangle = 0.0038$. For all sizes, the potential ϕ_{TGIP} is quasi-linear with a negative slope: the thermomigration effective force drives the cluster towards the cold region independently on its size.

Identifying all minima of $\Phi(x_0)$, we calculate $\phi_{TGIP}(\frac{1}{T})$ and perform a linear regression using the expression $\Phi_{TGIP}(\frac{1}{T}) = -\frac{Q}{T} + \Phi_0$. Q characterizes the thermomigration force that pushes the clusters towards the cold region. Table 3 reports values of Q for each cluster sizes as well as the cluster-substrate binding E^{0K}_{cl-sub} and the internal E^{0K}_{cl-cl} energies computed at 0 K and the expected slope $Q^{0K} = E^{0K}_{cl-cl} + E^{0K}_{cl-sub}$. The coefficient Q increases with cluster sizes. The measured coefficient Q is in good agreement, about 10% smaller with its theoretical value Q^{0K} at $0K$ validating the analysis of Sect. 4.2.4.

4.3.2. Random diffusion

In order to address the diffusive effects, we calculate the diffusion potential $\Phi_{Diff}(\frac{1}{T}) = \Phi(\frac{1}{T}) - \Phi_{TGIP}(\frac{1}{T})$.

Figure 9(a) shows Φ_{Diff} as a function of $\frac{1}{T}$. The function $\Phi_{Diff}(\frac{1}{T})$ is an oscillating function whose amplitude A_{Diff} increases with decreasing temperature. Figure 9(b) shows the amplitude A_{Diff} as a function of the inverse of the temperature. The amplitude A_{Diff} is related to the barrier of the cluster diffusion : as one can expect from entropic effect, this barrier decreases as the temperature increases. In order to address this temperature dependence, we perform a linear regression following the relation $A_{Diff}(\frac{1}{T}) = \frac{E_m}{T} - S$ with E_m the diffusion migration energy and S an entropy. Table 3 reports the values of E_m and S for each cluster. One should expect that the diffusion migration energy E_m corresponds to the activation energy E_a found when studying the cluster diffusion Table 2. For this reason, we have also reported in Table 3 the diffusion activation energy E_a. E_m and E_a differ but their ratio is about 0.8 except for the singular case $N = 2$. In the $N = 2$ case, the TI algorithm by constraining the x-position of the COM favors the observation of one of the diffusion mechanism, namely the one implying the rotation of the cluster with the smallest activation energy. Conversely, during the $N = 2$ cluster diffusion, we observe both rotation and translation of the cluster explaining the high diffusion activation energy.

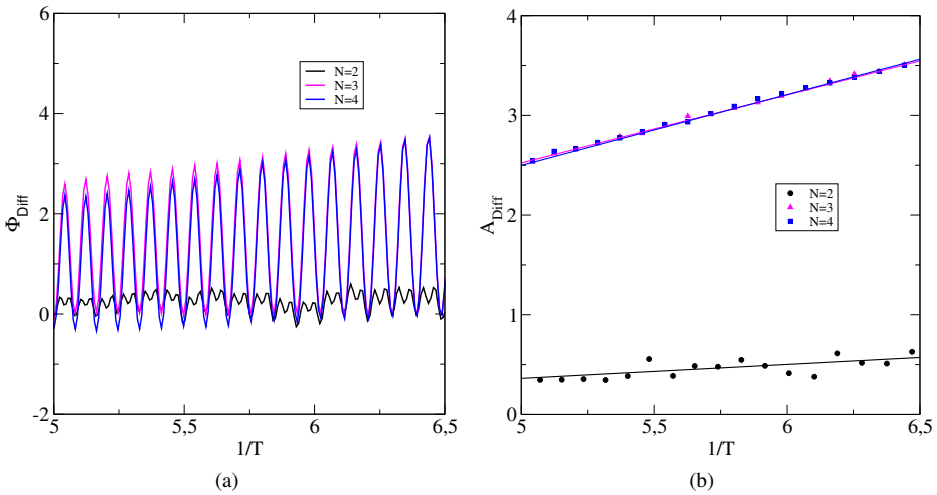

Figure 9: (a) Φ_{Diff} as a function of $\frac{1}{T}$. Φ_{Diff} is calculated according to $\Phi_{Diff}(\frac{1}{T}) = \Phi(\frac{1}{T}) - \Phi_{TGIP}(\frac{1}{T})$. (b) Amplitude A_{diff} of Φ_{Diff} as a function of the inverse of temperature and its linear regression following $A_{Diff}(\frac{1}{T}) = \frac{E_m}{T} - S$. The thermal gradient is $\langle \frac{\partial T}{\partial x} \rangle = 0.0038$.

4.3.3. Elastic effect

Figure 10(a) presents the thermodynamic potential for the $N = 3$ cluster as a function of the inverse of the temperature with a thermal gradient $\langle \frac{\partial T}{\partial x} \rangle = 0.0038$ for different values of the σ_{cl-cl} distance. The thermodynamic potential is again a linear function of $\frac{1}{T}$. Following our previous analysis, we extract from these curves the coefficient Q and the diffusion migration energy E_m. Figure 10(a) and 10(b) respectively show the coefficient Q and the diffusion migration energy

Table 3: Slopes Q, diffusion activation energies E_a, diffusion migration energy E_m and entropies S for the different clusters. E^{0K}_{cl-cl} and E^{0K}_{cl-sub} are the cluster internal and cluster-substrate binding energies at 0 K. The theoretical slope Q^{0K} at $0K$ is calculated according to $Q^{0K} = E^{0K}_{cl-cl} + E^{0K}_{cl-sub}$.

N	Q	E_a	E_m	S	E^{0K}_{cl-cl}	E^{0K}_{cl-sub}	Q^{0K}
2	11.80 ± 0.05	0.617	0.134	0.327	4.99	8.40	13.39
3	24.61 ± 0.02	0.838	0.684	0.901	14.99	12.58	27.57
4	39.34 ± 0.05	0.884	0.715	1.070	29.99	13.13	43.12

E_m for the cluster $N = 3$ as a function of the σ_{cl-cl} distance as well as their expected values Q^{0K} and E^{0K}_{mig} at 0K.

Our simulations do not exhibit a clear dependence of the slope Q on the σ_{cl-cl} distance: we observe that Q remains mainly independent on the σ_{cl-cl} distance. This result agrees with the dependence of the theoretical value Q^{0K} at 0K also reported Fig. 10(b): it only varies by 2.47% in Fig. 10(b) on the investigated range of values of σ_{cl-cl}. Clearly our simulations are not able to catch such a weak dependence.

Conversely, the diffusion migration energy E_m Fig. 10(b) has a clear maximum around $\sigma_{cl-cl} = 0.9$ and fully correlates with the dependence of the theoretical value E^{0K}_{mig} at 0K.

We conclude that the lattice mismatches have a weak influence on the thermomigration force, but a significant effect on the diffusion kinetic.

4.3.4. Interacting energy ϵ_{cl-cl}

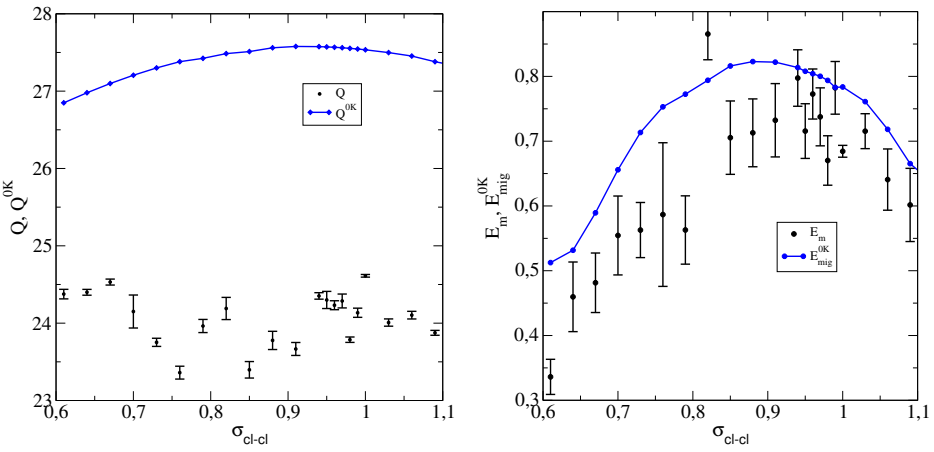

Figure 10: (a) Slope Q and theoretical slope Q^{0K} of ϕ_{TGIP} as a function of distance σ_{cl-cl}. (b) Diffusion migration energy E_m and migration energy E^{0K}_{mig} at 0K as a function of distance σ_{cl-cl}. $\langle \frac{\partial T}{\partial x} \rangle = 0.0038$

We finally investigate effects arising from variations of the interaction energy ϵ_{cl-cl} between the atoms in the cluster. In this study, we deliberately limit the accessible range $\epsilon_{cl-cl} \in [4-6]$ in order to prevent cluster dissociation on the simulation timescale.

We compute the thermodynamic potential of the $N = 3$ cluster as a function of the inverse of the temperature with the substrate simulated with a thermal gradient $\langle \frac{\partial T}{\partial x} \rangle = 0.0038$ for different

values of the ϵ_{cl-cl} energy. From the thermodynamic potential, we deduce the slope Q. Fig. 11 shows the coefficient Q as a function of the energy ϵ_{cl-cl} of the cluster $N = 3$. Q grows linearly with the energy ϵ_{cl-cl} with a slope of 2.44 and an intercept of 12.29. For comparison, the theoretical slope Q^{0K} calculated at 0 K is also displayed in Fig. 11: an linear regression gives a slope of 2.99 and an intercept of 12.54.

Both intercepts of Q and Q^{0K} are in excellent agreement and corresponds to the cluster-substrate binding energy at $0K$. The discrepancy between the slope of Q and Q^{0K} as a function of ϵ_{cl-cl} is of the order of 20% presumably due to entropic effects.

We conclude that the slope Q characterizing the thermomigration force that pushes the clusters towards the cold region agrees well with our interpretation as the sum of the cluster-substrate binding and cluster internal free energies.

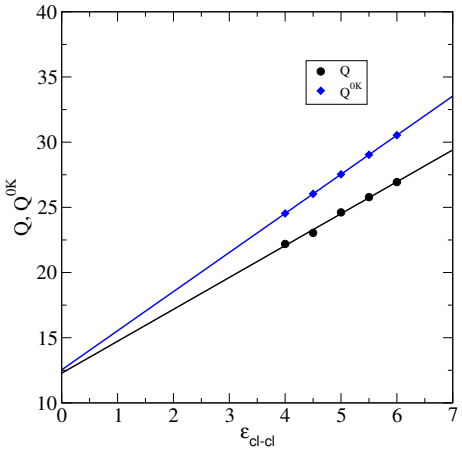

Figure 11: Slope Q and theoretical slope Q^{0K} at 0K and their linear fits (solid lines) as a function of binding energy ϵ_{cl-cl}.

5. Model for thermomigration

In order to relate the coefficient Q to the heat of transport involved in Eq. (1), we propose in this section to extend the kinetic model developed in Roux et al. [42, 43] to the case of clusters.

5.1. Model

The thermodynamic potential presents multiple metastable states: the cluster diffuses from one of these states to a neighbor one. We define Γ^+ (Γ^-) the probability per unit time that the cluster initially in a metastable state moves in the direction of increasing(decreasing) x. The generalization of the transition state theory to system with an inhomogeneous temperature provides Γ^+ and Γ^- [42]:

$$\begin{cases} \Gamma^+ &= \nu_+ e^{-[\phi(x_m+\frac{a}{2})-\phi(x_m)]} \\ \Gamma^- &= \nu_- e^{-[\phi(x_m+\frac{a}{2})-\phi(x_m+a)]} \end{cases} \tag{8}$$

With a the period of the thermodynamic potential and x_m represents the abscissa of a metastable site of the thermodynamic potential. We assume that the attempts frequencies are equals: $\nu_+ =$

$\nu_- = \nu_0$. Using results of Sect. 4.3, we get:

$$\begin{cases} \Phi(x_m) & = & -\frac{Q}{T(x_m)} + \Phi_0 \\ \Phi(x_m + \frac{a}{2}) & = & -\frac{Q}{T(x_m+\frac{a}{2})} + \frac{E_m - S\,T(x_m+\frac{a}{2})}{T(x_m+\frac{a}{2})} + \Phi_0 \\ \Phi(x_m + a) & = & -\frac{Q}{T(x_m+a)} + \Phi_0 \end{cases} \tag{9}$$

The average speed of the COM of the cluster thus writes:

$$\begin{aligned} \langle V \rangle &= a\left[\Gamma^+ - \Gamma^-\right] \\ &= \frac{D_0}{a} e^{\frac{Q-E_m}{T(x_m+\frac{a}{2})}} \left[e^{-\frac{Q}{T(x_m)}} - e^{-\frac{Q}{T(x_m+a)}} \right] \end{aligned} \tag{10}$$

Where we have used $D_0 = \nu_+ a^2 e^S$.

5.2. Link with Eq. (1)

If the thermal gradient is sufficiently small i.e. $Qa\frac{\partial \frac{1}{T}}{\partial x} \ll 1$, a Taylor expansion of Eq. (10) at the first order in $\frac{\partial \frac{1}{T}}{\partial x}$ yields:

$$\langle V \rangle = QD_0 e^{-\frac{E_m}{T(x_m)}} e^{\frac{Q-E_m}{2}\frac{\partial \frac{1}{T}}{\partial x}} \frac{\partial \frac{1}{T}}{\partial x} \tag{11}$$

$$\langle V \rangle = -D_0 e^{-\frac{E_m}{T(x_m)}} \frac{Q}{T(x_m)^2} e^{-\frac{Q-E_m}{2T(x_m)^2}\frac{\partial T}{\partial x}} \frac{\partial T}{\partial x} \tag{12}$$

Providing that $\frac{Q-E_m}{2T(x_m)^2}\frac{\partial T}{\partial x} \ll 1$, Eq. 12 is consistent with Eq. (1) where Q identifies with the heat of transport Q^*. Hence, the heat of transport Q^* is related to the sum of the cluster-substrate binding and cluster internal energies.

5.3. Comparison with molecular dynamic simulations

In order to compare the prediction of our model with the results of MD simulation, we compute the average trajectory of the cluster by solving the following differential equation:

$$\frac{dx}{dt} = \alpha \langle V \rangle \tag{13}$$

With α an adjustable parameter. We use the expression of the speed $\langle V \rangle$ given by Eq. (10): indeed, we have checked that the hypothesis $Qa\frac{\partial \frac{1}{T}}{\partial x} \ll 1$ yielding to Eq. (12) are not satisfied in our case.

In addition, Eq. (10) involves a diffusion migration energy E_m. As already mentioned, E_m should in principle identify with the diffusion activation energy E_a so that Eqs. (8) are compatible with results of the diffusion of a cluster on homogeneous substrate and $D(T) = D_0 e^{\frac{-E_m}{T}}$. However, E_m and E_a differ slightly for $N = 3$ and $N = 4$ and significantly for $N = 2$. Hence, in order to be as closed as possible from the diffusion of cluster, we used activation energies E_a in Eq. (10) instead of values of E_m deduced from the TI simulations: as already mentioned especially for the $N = 2$ cluster, some of diffusion mechanisms are not observed during the TI simulations, while they are during the free diffusion of the cluster on a substrate at homogeneous temperature.

Table 4 gathers the numeric values of the parameters that we use to solve Eq. (13). $T(x)$ is provided by a cubic regression of the temperature profile Fig. 2.

Table 4: Numerical values used to solve Eq. 13

N	a	Q	E_a	S	D_0
2	0.56	11.80	0.617	0.327	0.419
3	0.56	24.61	0.838	0.901	0.504
4	0.56	39.34	0.884	1.070	0.528

Figures 12(a), 12(b) and 12(c) show the trajectories calculated from Eq. (10) and the average trajectories calculated from MD simulations for a thermal gradient $\langle \frac{\partial T}{\partial x} \rangle = 0.0038$. The adjustable parameter α has been chosen so that both model and MD average trajectories agrees. We respectively use $\alpha = \frac{1}{8}, \frac{1}{8}$ and $\frac{1}{20}$ for the cluster $N = 2, 3$ and 4.

Hence our model predicts the thermomigration of clusters with a speed about one order of magnitude higher than what we observe in MD simulations. Though this result seems disappointing, we emphasize that it constitutes to our knowledge the first study providing a model of thermomigration of clusters with a direct quantitative comparison with MD simulations.

We have identified two possible ingredients of our model that could be improve and that are presumably responsible of the discrepancies with MD simulations. The first concerns the description of the kinetic of the cluster diffusion: indeed, we measure several kinetic properties that are inputs of our model and that significantly vary with the techniques used to determine them. Unfortunately, the diffusion of the clusters involves several atomic mechanisms whose kinetic characteristics are not easy to evaluate nor to identify. The second concerns the transition state theory. One one hand, the standard transition state theory is known to underestimate reaction rates since it neglects recrossing of reactive trajectories [59]: this underestimation is fully compatible with our finding of coefficients $\alpha < 1$. On the other hand, the reliability of the extension of the transition state theory to systems with inhomogeneous temperature Eq. (8) relies on a local thermodynamic equilibrium assumption [3]. This assumption is presumably true in the limit of an infinitely small thermal gradient, but its applicability to the thermal gradients used here might deserve a closer examination, which is clearly out of the scope of the present study.

6. Conclusion

In this manuscript, we have studied the thermomigration of clusters on crystalline surfaces. After evidencing the thermomigration of clusters through the examination of their trajectories, we have extended the thermodynamic integration method to measure the thermodynamic potential of clusters on substrate submitted to a thermal gradient. The determination of the thermodynamic potential driving the motion of the clusters on the surface allows to decorrelate the effective force induced by the thermal gradient from the diffusion. This analysis coupled to a kinetic model for thermomigration have shown that the heat of transport Q^* characterizing the thermomigration corresponds well with the sum of the cluster-substrate binding and cluster internal energies. Hence, we find that Q^* is always a positive quantity. In addition, we have shown that elastic effects weakly affect the heat of transport Q^*, so that a change of sign of Q^* does not seem reachable by changing the lattice mismatch between clusters and substrate. This analysis of elementary mechanisms of the thermomigration certainly deserves some extensions in order

[3] Especially, it assumes that the cluster is in equilibrium with the substrate along the transition.

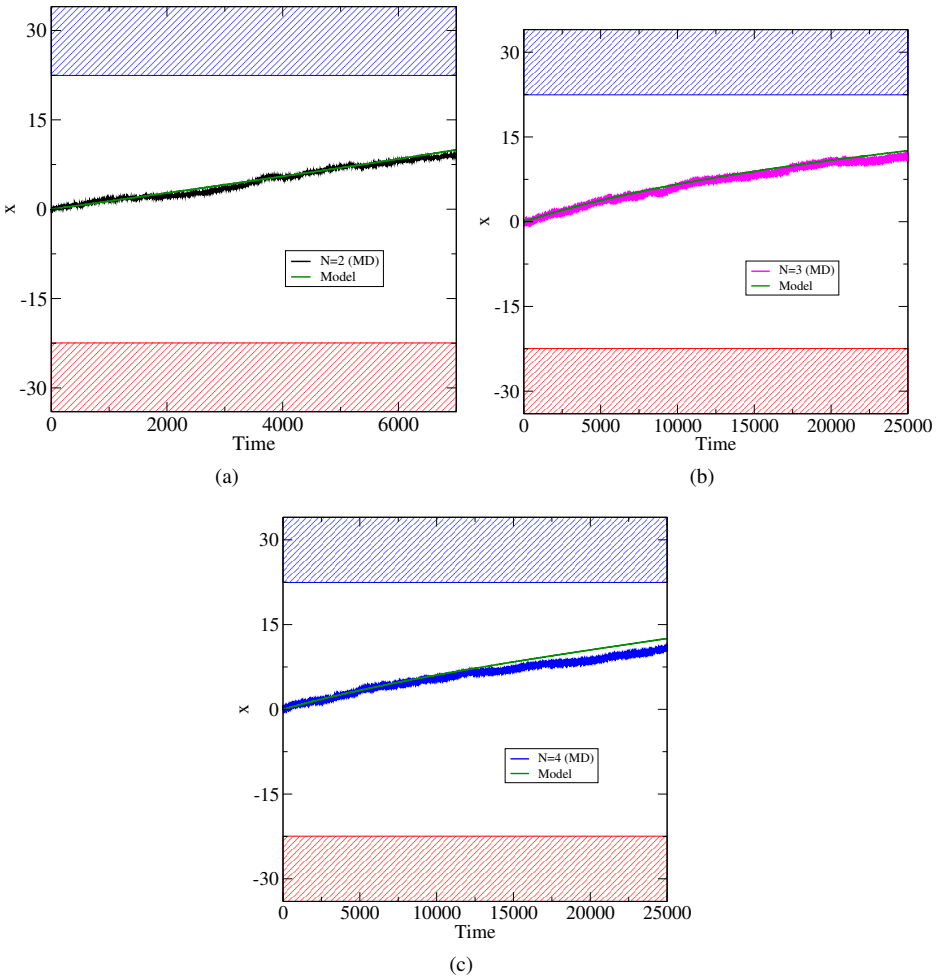

Figure 12: Trajectories calculated from the integration of Eq. 10 (solid green line) compared with the average MD trajectory for a thermal gradient $\langle \frac{\partial T}{\partial x} \rangle = 0.0038$. The red and blue hatched areas represent the hot and cold thermostated regions respectively. (a) For $N = 2$. (b) For $N = 3$. (c) For $N = 4$

to address cases where the transfer of momentum from phonons presumably plays a more important role in the thermomigration. Especially, analyzing the thermomigration of clusters on graphene [28, 34], which is characterized by weak binding energies, may help to demonstrate the role and to quantify this transfer of momentum from phonons.

Acknowledgement

This work was performed using HPC resources from CALMIP (Grant No.2016-P21031).

Data availability statement

The data that support the findings of this study are available from the corresponding author, [author initials], upon reasonable request.

Appendix A. Thermodynamic integration for a cluster submitted to a thermal gradient

In this section, we develop the thermodynamic integration (TI) method for a cluster on a substrate subjected to a thermal gradient.

Let's M and N be the number of atoms in the cluster and in the substrate. Clusters and substrate atoms indices will be respectively k or $l \in \{1, .., M\}$ and i or $j \in \{1, .., N\}$. Clusters (substrate) atom $k(i)$ has a mass $m_k(m_i)$. $\frac{\sum_k^M x_k}{M}$ designs the x-component of the cluster COM.

Assuming local thermal equilibrium, the probability of presence of the cluster with its COM abscissa x_0 is defined as:

$$p(x_0) = \frac{Z_r(x_0)}{Z} \tag{A.1}$$

with Z the partition function of the system. $Z_r(x_0)$ represents the reduced partition function of the system (substrate+cluster), i.e. a partition function calculated on a set of microstates for which the COM of the cluster has the abscissa x_0.

The partition function and the reduced partition function write [57, 58] as:

$$Z = \frac{1}{h^{3M+3N}} \int e^{\left[-\int \frac{\mathcal{H}(\vec{r})}{T(\vec{r})} d^3\vec{r}\right]} \prod_{k=1}^{M} d^3\vec{r}_k d^3\vec{p}_k \prod_{i=1}^{N} d^3\vec{r}_i d^3\vec{p}_i \tag{A.2}$$

$$Z_r(x_0) = \frac{1}{h^{3M+3N}} \int \delta\left(\frac{\sum_k^M x_k}{M} - x_0\right) e^{\left[-\int \frac{\mathcal{H}(\vec{r})}{T(\vec{r})} d^3\vec{r}\right]} \prod_{k=1}^{M} d^3\vec{r}_k d^3\vec{p}_k{}^3 \prod_{i=1}^{N} d^3\vec{r}_i d^3\vec{p}_i \tag{A.3}$$

Where the microscopic many-body Hamiltonian density $\mathcal{H}(\vec{r})$ of the system is defined as [57, 58]:

$$\begin{aligned} \mathcal{H}(\vec{r}) = & \sum_k^M \delta(\vec{r}_k - \vec{r}) \left[\frac{p_k^2}{2m} + \frac{1}{2} \sum_i^N E_{LJ}(\vec{r}_k, \vec{r}_i) + \sum_{l \neq k}^M \frac{1}{2} E_{LJ}(\vec{r}_k, \vec{r}_l) \right] \\ & + \sum_i^N \delta(\vec{r}_i - \vec{r}) \left[\frac{p_i^2}{2m_i} + \frac{1}{2} \sum_k^M E_{LJ}(\vec{r}_k, \vec{r}_i) + \sum_{j \neq i}^N \frac{1}{2} E_{LJ}(\vec{r}_i, \vec{r}_j) \right] \end{aligned} \tag{A.4}$$

In our system, the temperature only depends on the x-position, so that we can write $T(\vec{r}) = T(x)$. From Eq. (A.4), we deduce:

$$\begin{aligned}\int \frac{\mathcal{H}(\vec{r})}{T(\vec{r})} d^3\vec{r} &= \frac{1}{2}\sum_{k\neq l}^{M} E_{LJ}(\vec{r_k},\vec{r_l})\left[\frac{1}{T(x_k)}+\frac{1}{T(x_l)}\right] \\ &+ \sum_{k}^{M}\frac{p_k^2}{2m_k T(x_k)} + \frac{1}{2}\sum_{i}^{N}\sum_{k}^{M} E_{LJ}(\vec{r_k},\vec{r_i})\left[\frac{1}{T(x_k)}+\frac{1}{T(x_i)}\right] \\ &+ \sum_{i}^{N}\frac{p_i^2}{2m_i T(x_i)} + \frac{1}{2}\sum_{j\neq i} E_{LJ}(\vec{r_i},\vec{r_j})\left[\frac{1}{T(x_i)}+\frac{1}{T(x_j)}\right] \end{aligned} \tag{A.5}$$

The reduced partition function finally reads:

$$\begin{aligned} Z_r(x_0) &= \frac{1}{h^{3M+3N}}\int \delta(\frac{\sum^M x_k}{M}-x_0)\prod_{k=1}^{M} d^3\vec{r_k} d^3\vec{p_k}^{\,3}\prod_{i=1}^{N} d^3\vec{r_i} d^3\vec{p_i} \\ &\quad e^{-\left[\sum_k^M \sum_{l\neq k}^M \frac{1}{2}E_{LJ}(\vec{r_k},\vec{r_l})\left[\frac{1}{T(x_k)}+\frac{1}{T(x_l)}\right]\right]} \\ &\quad e^{-\left[\sum_k^M \frac{p_k^2}{2mT(x_k)}+\frac{1}{2}\sum_i^N\sum_k^M\left[E_{LJ}(\vec{r_k},\vec{r_i})\left[\frac{1}{T(x_k)}+\frac{1}{T(x_i)}\right]\right]\right]} \\ &\quad e^{-\left[\sum_i^N \frac{{p_i}^2}{2m_i T(x_i)}+\sum_i^N\sum_{j\neq i}^N \frac{1}{2}E_{LJ}(\vec{r_i},\vec{r_j})\left[\frac{1}{T(x_i)}+\frac{1}{T(x_j)}\right]\right]} \end{aligned} \tag{A.6}$$

Calling $\vec{r}_m = (x_m, y_m, z_m) = \frac{\sum^M \vec{r_k}}{M}$ the cluster COM, we introduce the reduced coordinates $\vec{r'}_k = \vec{r}_k - \vec{r}_m$:

$$\begin{aligned} Z_r(x_0) &= \frac{M^3}{h^{3M+3N}}\int \delta(x_m-x_0)\delta(\sum_k^M \vec{r_k'})d^3\vec{r_m}\prod_{k=1}^{M} d^3\vec{r_k} d^3\vec{p_k}\prod_{i=1}^{N} d^3\vec{r_i} d^3\vec{p_i} \\ &\quad e^{-\left[\sum_k^M \sum_{l\neq k}^M \frac{1}{2}E_{LJ}(\vec{r_k'}+\vec{r_m},\vec{r_l'}+\vec{r_m})\left[\frac{1}{T(x_k'+x_m)}+\frac{1}{T(x_l'+x_m)}\right]\right]} \\ &\quad e^{-\left[\sum_k^M \frac{{p_k}^2}{2mT(x_k'+x_m)}+\frac{1}{2}\sum_i^N\sum_k^M E_{LJ}(\vec{r_k'}+\vec{r_m},\vec{r_i})\left[\frac{1}{T(x_k'+x_m)}+\frac{1}{T(x_i)}\right]\right]} \\ &\quad e^{-\left[\sum_i^N \frac{{p_i}^2}{2m_i T(x_i)}+\sum_i^N\sum_{j\neq i}^N \frac{1}{2}E_{LJ}(\vec{r_i},\vec{r_j})\left[\frac{1}{T(x_i)}+\frac{1}{T(x_j)}\right]\right]} \end{aligned} \tag{A.7}$$

Integrating over dx_m, we get:

$$Z_r(x_0) = \frac{M^3}{h^{3M+3N}}\int \delta(\sum_k^M \vec{r_k'})e^{-\kappa(x_0)}dy_m dz_m\prod_{k=1}^{M} d^3\vec{r_k} d^3\vec{p_k}\prod_{i=1}^{N} d^3\vec{r_i} d^3\vec{p_i} \tag{A.8}$$

with

$$\begin{aligned}\kappa(x_0) &= \sum_{k}^{M}\sum_{l\neq k}^{M}\frac{1}{2}E_{LJ}(\vec{r_k'}+\vec{r_m^0},\vec{r_l'}+\vec{r_m^0})\left[\frac{1}{T(x_k'+x_0)}+\frac{1}{T(x_l'+x_0)}\right] \\ &+ \sum_{k}^{M}\frac{{p_k}^2}{2mT(x_k'+x_0)} + \frac{1}{2}\sum_{i}^{N}\sum_{k}^{M} E_{LJ}(\vec{r_k'}+\vec{r_m^0},\vec{r_i})\left[\frac{1}{T(x_k'+x_0)}+\frac{1}{T(x_i)}\right] \\ &+ \sum_{i}^{N}\frac{{p_i}^2}{2m_i T(x_i)} + \sum_{i}^{N}\sum_{j\neq i}^{N}\frac{1}{2}E_{LJ}(\vec{r_i},\vec{r_j})\left[\frac{1}{T(x_i)}+\frac{1}{T(x_j)}\right] \end{aligned} \tag{A.9}$$

$\vec{r_m^0} = (x_0, y_m, z_m)$ the position of the cluster's COM.

Noticing that the terms $E_{LJ}(\vec{r_k}' + \vec{r_m^0}, \vec{r_l}' + \vec{r_m^0}) = E_{LJ}(\left|\vec{r_k} - \vec{r_l}\right|) = E_{LJ}(\vec{r_k}, \vec{r_l})$ do not depend on x_0, From equations (A.8) and (A.9), we get:

$$
\begin{aligned}
-\frac{\partial Z_r}{\partial x_0}(x_0) &= \frac{M^3}{h^{3M+3N}} \int \delta(\sum_k^M \vec{r_k}') e^{-\kappa(x_0)} dy_m dz_m \prod_{k=1}^{M} d^3\vec{r_k} d^3\vec{p_k} \prod_{i=1}^{N} d^3\vec{r_i} d^3\vec{p_i} \\
&\left(\sum_k^M \sum_{l\neq k}^M \frac{1}{2} \frac{\partial\left(\frac{1}{T(x_k'+x_0)} + \frac{1}{T(x_l'+x_0)}\right)}{\partial x_0} E_{LJ}(\vec{r_k}, \vec{r_l}) \right. \\
&+ \sum_k^M \frac{{p_k}^2}{2m_k} \frac{\partial\left(\frac{1}{T(x_k'+x_0)}\right)}{\partial x_0} \\
&+ \frac{1}{2} \sum_i^N \sum_k^M \frac{\partial\left(E_{LJ}(\vec{r_k}' + \vec{r_m^0}, \vec{r_i})\right)}{\partial x_0} \left[\frac{1}{T({x_k}' + x_0)} + \frac{1}{T(x_i)} \right] \\
&\left. + \frac{1}{2} \sum_i^N \sum_k^M \frac{\partial\left(\frac{1}{T({x_k}'+x_0)}\right)}{\partial x_0} E_{LJ}(\vec{r_k}' + \vec{r_m^0}, \vec{r_i}) \right)
\end{aligned}
\tag{A.10}
$$

In the following we use the notations $E_{LJ}(k \leftrightarrow sub) = \sum_i^N E_{LJ}(\vec{r_k}, \vec{r_i})$ the interaction of cluster atom k with the substrate and $F_x(i \to k) = -\frac{\partial}{\partial x_0}\left(E_{LJ}(\vec{r_k}, \vec{r_i})\right)$ the x-component of the force exerted by the substrate atom i on the cluster atom k.

The derivative of the thermodynamic potential is hence:

$$
\begin{aligned}
\frac{\partial \Phi}{\partial x}(x_0) &= -\frac{\frac{\partial Z_r}{\partial x_0}}{Z_r}(x_0) \\
&= -\left\langle \sum_i^N \sum_k^M \frac{F_x(i \to k)}{2} \left[\frac{1}{T(x_k)} + \frac{1}{T(x_i)} \right] \right\rangle_{x_0} \\
&+ \left\langle \sum_k^M \frac{\partial\left(\frac{1}{T(x_k)}\right)}{\partial x_0} \left[\frac{{p_k}^2}{2m} + \frac{E_{LJ}(k \leftrightarrow sub)}{2} \right] \right\rangle_{x_0} \\
&+ \left\langle \sum_k^M \sum_{l\neq k}^M \frac{1}{2} \frac{\partial\left(\frac{1}{T(x_k)} + \frac{1}{T(x_l)}\right)}{\partial x_0} E_{LJ}(\vec{r_k}, \vec{r_l}) \right\rangle_{x_0}
\end{aligned}
\tag{A.11}
$$

where $\langle . \rangle_{x_0}$ denotes the average over all microstates compatible with the constrain $x_0 = \frac{\sum_k^M x_k}{M}$. Eq. (A.11) can be estimated from MD simulations and $\Phi(x_0)$ deduces by numerical integration.

References

[1] C. Ludwig, Lehrbuch der Physiologie des Menschen: Physiologie der Atome, der Aggregatzustände, der Nerven und Muskeln. Erster Band, no. vol. 1, C. F. Winter, 1858.
URL `https://books.google.fr/books?id=ZS5WvAEACAAJ`

[2] C. Soret, Au point de vue de sa concentration une dissolution saline primitivement homogène dont deux parties sont portées à des temperatures différentes, Archives des Sciences Physiques et Naturelles de Geneve, 2 (1879) 48. doi:10.1051/jphystap:018800090033101.
[3] J. Tyndall, On haze and dust, Nature 1 (1870) 339–342. doi:10.1038/001339a0.
[4] R. J. Strutt, Iv. on the dark plane which is formed over a heated wire in dusty air, Proceedings of the Royal Society of London 34 (220-223) (1883) 414–418. doi:10.1098/rspl.1882.0059.
[5] H. Huntington, Driving forces for thermal mass transport, Journal of Physics and Chemistry of Solids 29 (9) (1968) 1641–1651. doi:https://doi.org/10.1016/0022-3697(68)90106-6.
[6] W. G. Pfann, Zone melting, Wiley series on the science and technology of materials, Wiley, 1958.
[7] E. Buchin, Y. Denisenko, Use of thermomigration in mems technology, in: K. A. Valiev, A. A. Orlikovsky (Eds.), SPIE Proceedings, Vol. 6260, SPIE, 2006, pp. 62601L–62601L. doi:10.1117/12.683500.
[8] M. Eslamian, Z. Saghir, Thermodiffusion applications in mems, nems and solar cell fabrication by thermal metal doping of semiconductors, Fluid Dynamics and Materials Processing 8 (2012) 353–380. doi:10.3970/fdmp.2012.008.353.
[9] J. Janek, H. Timm, Thermal diffusion and Soret effect in (U,Me)O $_{2+\delta}$: the heat of transport of oxygen, Journal of Nuclear Materials 255 (2) (1998) 116–127. doi:10.1016/S0022-3115(98)00037-3.
[10] D. Peterson, Seon Jin Kim, Thermotransport of hydrogen in niobium and tantalum as a function of concentration, Journal of the Less Common Metals 141 (2) (1988) 249–259. doi:10.1016/0022-5088(88)90411-0.
[11] M. Uz, O. Carlson, Thermotransport and diffusion of carbon in vanadium and vanadium-titanium alloys, Journal of the Less Common Metals 116 (2) (1986) 317–332. doi:10.1016/0022-5088(86)90665-X.
[12] B. Ernst, G. Frohberg, K. Kraatz, H. Wever, Bulk electro- and thermotransport in al, in: Diffusion in Materials DIMAT 1996, Vol. 143 of Defect and Diffusion Forum, Trans Tech Publications Ltd, 1997, pp. 1649–1654. doi:10.4028/www.scientific.net/DDF.143-147.1649.
[13] P. A. E. Schoen, J. H. Walther, S. Arcidiacono, D. Poulikakos, P. Koumoutsakos, Nanoparticle traffic on helical tracks: Thermophoretic mass transport through carbon nanotubes, Nano Letters 6 (9) (2006) 1910–1917. doi:10.1021/nl060982r.
[14] P. A. E. Schoen, J. H. Walther, D. Poulikakos, P. Koumoutsakos, Phonon assisted thermophoretic motion of gold nanoparticles inside carbon nanotubes, Applied Physics Letters 90 (25) (2007) 253116. doi:10.1063/1.2748367.
[15] A. Barreiro, R. Rurali, E. R. Hernández, J. Moser, T. Pichler, L. Forró, A. Bachtold, Subnanometer motion of cargoes driven by thermal gradients along carbon nanotubes, Science 320 (5877) (2008) 775–778. doi:10.1126/science.1155559.
[16] H. Somada, K. Hirahara, S. Akita, Y. Nakayama, A molecular linear motor consisting of carbon nanotubes, Nano Letters 9 (1) (2009) 62–65. doi:10.1021/nl802323n.
[17] e. a. De-Gang Xie, Controlled growth of single-crystalline metal nanowires via thermomigration across a nanoscale junction, Nature Communications, 10 (2019) 4478. doi:10.1038/s41467-019-12416-x.
[18] F. Leroy, A. El Barraj, F. Cheynis, P. Müller, S. Curiotto, Determination of the thermomigration force on adatoms, Phys. Rev. Lett. 131 (2023) 116202. doi:10.1103/PhysRevLett.131.116202.
[19] S. Curiotto, N. Combe, P. Müller, A. El Barraj, N. Abu Dahech, F. Cheynis, O. Pierre-Louis, F. Leroy, Surface thermomigration of 2d voids, Applied Physics Letters 125 (12) (2024) 121601. arXiv:https://pubs.aip.org/aip/apl/article-pdf/doi/10.1063/5.0228961/20161422/121601_1_5.0228961.pdf, doi:10.1063/5.0228961.
[20] Q.-W. Hou, B.-Y. Cao, Z.-Y. Guo, Thermal gradient induced actuation in double-walled carbon nanotubes, Nanotechnology 20 (49) (2009) 495503. doi:10.1088/0957-4484/20/49/495503.
[21] V. R. Coluci, V. S. Tim'oteo, D. S. Galvão, Thermophoretically driven carbon nanotube oscillators, Applied Physics Letters 95 (2009) 253103. doi:10.48550/arXiv.1001.0651.
[22] J. Leng, Z. Guo, H. Zhang, T. Chang, X. Guo, H. Gao, Negative thermophoresis in concentric carbon nanotube nanodevices, Nano Letters 16 (10) (2016) 6396–6402. doi:10.1021/acs.nanolett.6b02815.
[23] R. Rurali, E. Hernández, Thermally induced directed motion of fullerene clusters encapsulated in carbon nanotubes, Chemical Physics Letters 497 (1) (2010) 62 – 65. doi:https://doi.org/10.1016/j.cplett.2010.07.081.
[24] W. Yao, C. Basaran, Damage mechanics of electromigration and thermomigration in lead-free solder alloys under alternating current: An experimental study, International Journal of Damage Mechanics 23 (2013) 203–221. doi:10.1177/1056789513488396.
[25] A. V. Savin, O. I. Savina, Thermophoresis of Single Atomic Particles in Open Nanotubes, Physics of the Solid State 63 (5) (2021) 811–818. doi:10.1134/S106378342104020X.
[26] A. V. Savin, Y. A. Kosevich, A. Cantarero, Semiquantum molecular dynamics simulation of thermal properties and heat transport in low-dimensional nanostructures, Phys. Rev. B 86 (2012) 064305. doi:10.1103/PhysRevB.86.064305.
[27] M. Becton, X. Wang, Thermal gradients on graphene to drive nanoflake motion, J. Chem. Theory Comput 10

(2014) 722. doi:10.1021/ct400963d.
[28] E. Panizon, R. Guerra, E. Tosatti, Ballistic thermophoresis of adsorbates on free-standing graphene, Proceedings of the National Academy of Sciences 114 (2017) E7035. doi:10.1073/pnas.1708098114.
[29] R. Rajegowda, S. K. Kannam, R. Hartkamp, S. P. Sathian, Thermophoretically driven water droplets on graphene and boron nitride surfaces, Nanotechnology 29 (21) (2018) 215401. doi:10.1088/1361-6528/aab3a3.
[30] A. V. Savin, Friction, mobility, and thermophoresis of carbon nanoparticles on a graphene sheet, Phys. Rev. B 106 (2022) 205410. doi:10.1103/PhysRevB.106.205410.
[31] Z.-Y. Guo, Q.-W. Hou, B.-Y. Cao, A Novel Thermal Driving Force for Nanodevices, Journal of Heat Transfer 134 (5) (2012) 051010. doi:10.1115/1.4005640.
[32] Q. Zhu, S. Zhao, C. Deng, X. An, K. Song, S. Mao, J. Wang, In situ atomistic observation of grain boundary migration subjected to defect interaction, Acta Materialia 199 (2020) 42 – 52. doi:https://doi.org/10.1016/j.actamat.2020.08.021.
[33] R. L. Zhang, S. Y. Li, Y. Li, M. F. Wang, Controlled mass transportation on nanotubes by strain and thermal gradient: A molecular dynamics study, Journal of Nano Research 74 (2022) 97 – 107. doi:10.4028/p-wj60p1.
[34] Q. Sun, J. Leng, T. Chang, Ring-shaped nanomotors of heterojuncted carbon boron-nitride nanotubes, Computational Materials Science 233 (2024) 112725. doi:https://doi.org/10.1016/j.commatsci.2023.112725.
[35] L. Onsager, Reciprocal relations in irreversible processes. i., Phys. Rev. 37 (1931) 405–426. doi:10.1103/PhysRev.37.405.
[36] J. A. Brinkman, The effect of temperature gradients on diffusion in crystals, Phys. Rev. 93 (1954) 345–345. doi:10.1103/PhysRev.93.345.
[37] G. Schottky, A theory of thermal diffusion based on the lattice dynamics of a linear chain, Physica Status Solidi (b) 8 (1) (1965) 357–368. doi:https://doi.org/10.1002/pssb.19650080135.
[38] K. Wirtz, On the kinetic theory of thermodiffusion in crystal lattices, Physik. Z 44 (1943) 221–231.
[39] A. D. LeClaire, Some predicted effects of temperature gradients on diffusion in crystals, Phys. Rev. 93 (1954) 344–344. doi:10.1103/PhysRev.93.344.
[40] W. Shockley, Some predicted effects of temperature gradients on diffusion in crystals, Phys. Rev. 93 (1954) 345–346. doi:10.1103/PhysRev.93.345.2.
[41] A. R. Allnati, S. A. Rice, On the Dynamical Theory of Diffusion in Crystals. V. Random-Walk Treatment of the Heat of Transport, The Journal of Chemical Physics 33 (2) (1960) 573–578. doi:10.1063/1.1731187.
[42] A. Roux, N. Combe, Thermal mass transport mechanism of an adatom on a crystalline surface, Phys. Rev. B 108 (2023) 115410. doi:10.1103/PhysRevB.108.115410.
[43] A. Roux, N. Combe, Erratum: Thermal mass transport mechanism of an adatom on a crystalline surface [phys. rev. b 108, 115410 (2023)], Phys. Rev. B 110 (2024) 119902. doi:10.1103/PhysRevB.110.119902.
[44] A. Roux, Thermomigration at the nanometer scale, Ph.D. thesis, University of Paul Sabatier Toulouse III (2024).
[45] A. P. Thompson, H. M. Aktulga, R. Berger, D. S. Bolintineanu, W. M. Brown, P. S. Crozier, P. J. in 't Veld, A. Kohlmeyer, S. G. Moore, T. D. Nguyen, R. Shan, M. J. Stevens, J. Tranchida, C. Trott, S. J. Plimpton, LAMMPS - a flexible simulation tool for particle-based materials modeling at the atomic, meso, and continuum scales, Comp. Phys. Comm. 271 (2022) 108171. doi:10.1016/j.cpc.2021.108171.
[46] J. E. Lennard-Jones, Cohesion, Proceedings of the Physical Society 43 (5) (1931) 461. doi:10.1088/0959-5309/43/5/301.
[47] A. Márquez, P. B. Balbuena, Molecular dynamics study of graphite/electrolyte interfaces, Journal of The Electrochemical Society 148 (6) (2001) A624. doi:10.1149/1.1372216.
[48] M. Allen, D. Tildesley, Computer Simulation of Liquids, Computer Simulation of Liquids, Clarendon Press, 1987.
[49] E. A. Mastny, J. J. de Pablo, Melting line of the lennard-jones system, infinite size, and full potential, The Journal of Chemical Physics 127 (10) (2007) 104504. doi:10.1063/1.2753149.
[50] P. Guan, D. R. Mckenzie, B. A. Pailthorpe, Md simulations of ag film growth using the lennard-jones potential, J. Phys.: Condens. Matter 8 (1996) 8753–8762. doi:10.1088/0953-8984/8/45/011.
[51] P. Chantrenne, J.-L. Barrat, Finite size effects in determination of thermal conductivities: Comparing molecular dynamics results with simple models, J. Heat Transfer 126 (2004) 577–585. doi:10.1115/1.1777582.
[52] N. G. H. Jean-Philippe M. Peraud, Colin D. Landon, Monte carlo methods for solving the boltzmann transport equation, Annual Review of Heat Transfer 17 (2014) 205–265. doi:10.1615/AnnualRevHeatTransfer.2014007381.
[53] P. L. Kapitza, The study of heat transfer in helium ii, 1971. doi:10.1016/B978-0-08-015816-7.50014-6.
[54] E. T. Swartz, R. O. Pohl, Thermal boundary resistance, Rev. Mod. Phys. 61 (1989) 605–668. doi:10.1103/RevModPhys.61.605.
[55] D. Sun, X. Gong, Cluster on the fcc(111) surface: structure, stability and diffusion, Surface Science 445 (1) (2000) 41–48. doi:10.1016/S0039-6028(99)01035-3.
[56] P. Deltour, Etude de la diffusion d'un agrégat sur une surface cristalline, Ph.D. thesis, Université claude Bernard - Lyon 1, thèse de doctorat dirigée par Barrat, Jean-Louis Sciences Lyon 1 1998 (1998).

URL http://www.theses.fr/1998LYO19007
[57] H. Mori, Statistical-mechanical theory of transport in fluids, Phys. Rev. 112 (1958) 1829–1842. doi:10.1103/PhysRev.112.1829.
[58] P. Anzini, G. M. Colombo, Z. Filiberti, A. Parola, Thermal forces from a microscopic perspective, Phys. Rev. Lett. 123 (2019) 028002. doi:10.1103/PhysRevLett.123.028002.
[59] P. Hänggi, P. Talkner, M. Borkovec, Reaction-rate theory: fifty years after kramers, Rev. Mod. Phys. 62 (2) (1990) 251–341. doi:10.1103/RevModPhys.62.251.